Lab on a Chip

PAPER

View Article Online
View Journal | View Issue

Cite this: *Lab Chip*, 2016, **16**, 1430

Direct 3D-printing of cell-laden constructs in microfluidic architectures†

Justin Liu,[a] Henry H. Hwang,[b] Pengrui Wang,[a] Grace Whang[b] and Shaochen Chen*[ab]

Received 1st February 2016,
Accepted 8th March 2016

DOI: 10.1039/c6lc00144k

www.rsc.org/loc

Microfluidic platforms have greatly benefited the biological and medical fields, however standard practices require a high cost of entry in terms of time and energy. The utilization of three-dimensional (3D) printing technologies has greatly enhanced the ability to iterate and build functional devices with unique functions. However, their inability to fabricate within microfluidic devices greatly increases the cost of producing several different devices to examine different scientific questions. In this work, a variable height micromixer (VHM) is fabricated using projection 3D-printing combined with soft lithography. Theoretical and flow experiments demonstrate that altering the local *z*-heights of VHM improved mixing at lower flow rates than simple geometries. Mixing of two fluids occurs as low as 320 μL min^{-1} in VHM whereas the planar zigzag region requires a flow rate of 2.4 mL min^{-1} before full mixing occurred. Following device printing, to further demonstrate the ability of this projection-based method, complex, user-defined cell-laden scaffolds are directly printed inside the VHM. The utilization of this unique ability to produce 3D tissue models within a microfluidic system could offer a unique platform for medical diagnostics and disease modeling.

Introduction

As trends toward improving global public health and point-of-care technologies gain traction in research and development, Lab-on-a-Chip (LoC) technologies designed for microfluidic manipulation of biological fluids and/or multi-species mixtures continue to be active areas of research.[1–3] LoC devices are especially attractive due to use of microfluidics to integrate multiple fluidic and analytical processes, giving them many-fold advantages[4] over traditional laboratory functions, such as: 1) reduction in sample processing runtime, resource cost, and volume, 2) simplicity of assay deployment and user training, and 3) multiplexability and batch processing capabilities.

One function crucial to microfluidic LoC devices is the ability to mix and manipulate disparate substances to any desired degree.[5] However, microfluidic flow conditions are typically laminar and uniaxial, resulting in mixing being dominated by molecular diffusion rather than convective mass transfer.[4] Consequently, cells, particles, or other flowing species present tend to stay in their own fluidic streamlines, minimizing interactions with other species and/or critical structural features of the LoC device.[4] Current research in microfluidic mixers has yielded results in the form of active micromixers, which rely on externally-supplied energy and equipment to drive mixing, thus adding complexity to their design, construction, and operation.[6] Alternatively, passive micromixers' only energy requirement comes from the initial fluidic driver, otherwise utilizing device-level structural features for enhanced diffusion and advective mixing.[5] While planar passive mixers have been successful in microfluidic mixing due to their simplicity of design and construction, there is potential to improve efficiency by extending feature geometries into the third dimension such as with three-dimensional (3D) passive micromixers,[7–9] but these can be onerous to manufacture due to limitations in current manufacturing methods.

The current gold standard in microfluidic device fabrication is soft lithography, a technique where a 'soft' material like polydimethylsiloxane (PDMS) is used to cast a 3D master molding with micrometer-scale features.[10] Traditional methods for 3D master mold fabrication often involve cleanroom-gated silicon wafer-based photolithography, where multiple high-resolution photomasks must be sequentially-aligned and exposed to incrementally build up layers of photoresist into the desired 3D structure.[10–12] Photolithography tends to be tedious, challenging, and expensive in terms of time, training, and resources, thus limiting final device quality and reproducibility.[13,14] Within this context, 3D-printing is emerging as a more preferable method for rapid prototyping of microfluidic device designs and concepts.[15–22] However, traditional additive manufacturing techniques, such as extrusion-based[23] or inkjet-based 3D-printing[18] suffer from such limitations as poor feature resolution, limited build

[a] *Materials Science and Engineering Program, University of California, San Diego, CA 92093, USA. E-mail: chen168@eng.ucsd.edu*
[b] *Department of NanoEngineering, University of California, San Diego, CA 92093, USA*
† Electronic supplementary information (ESI) available. See DOI: 10.1039/c6lc00144k

volumes, and long runtimes. Particularly for tissue engineering applications, microfluidic devices fabricated with these methods tend to leave their users with limited monolayer culture analysis or bulk gel studies.[24,25] Recently, simple 3D structures have been printed within a microfluidic device using extrusion-based manufacturing techniques using three bioinks.[22] However, the user must seal the microfluidic device before use, preventing any changes to the printed geometry and requiring the user to fabricate new devices for future 3D applications. 3D-printed modular microfluidic devices have also been designed,[26] with the ability to pick and choose various applications, like mixing. However, for tissue engineering applications, users will be limited to thermal gelation of bulk gels within the microfluidic device. To further extend on this new emerging field of 3D tissue engineering, there is large potential in incorporating 3D tissue constructs with defined architectures into a microfluidic device to not only minimize waste of costly resources, but to also enable studies of cell behavior and metabolic output in real time under flow.

Therefore, we present the application of digital micromirror device (DMD)-based printing in the construction of a novel 3D-printer enabled variable height micromixer (VHM). DMD-based printing utilizes an array of millions of individually-controllable micromirrors to project a 2D image onto a moving plane of photopolymerizable prepolymer solution, thereby allowing production of 3D high-resolution microstructures.[27–30] An advanced technology, micro-continuous optical printing (μCOP) utilizes a DMD and dynamically projects different images as a stage moves a prepolymer solution vertically through the system's optical focal plane, rapidly creating complex 3D microstructures.[17,31–38] This grants the ability to rapidly prototype and iterate through master mold generations without the time and resource-intensive issues that plague other 3D-printing techniques. In this report, the VHM design incorporates rectangular columns of varying heights within zigzagging block-shaped fluidic elements that lead to an optically-clear chamber for later *in situ* fabrication of structures. The mixing performance of this device was investigated experimentally with fluorescence microscopy for a range of volumetric flow rates ranging from 20 μL min^{-1} to 2.4 mL min^{-1}. Then, capitalizing on the μCOP system's ability to fabricate structures without physically contacting the printing medium, we demonstrate the ability to fabricate a complex 3D scaffold within an already-completed microfluidic device, using on-chip mixing of a live cell suspension with a prepolymer solution. In addition to its effective mixing capability, this device showcases the capacity to facilely construct complex 3D microfluidic devices that enable direct study of how factors such as fluid flow and microarchitecture can affect cell behavior.

Experimental

Prepolymer solution preparation

Polyethylene glycol diacrylate (PEGDA, MW ~ 700), 2-hydroxy-4-methoxy-benzophenon-5-sulfonic acid (HMBS), 2,2,6,6-tetramethylpiperidine 1-oxyl (TEMPO, free-radical quencher) were purchased from Sigma-Aldrich. Photoinitiator Irgacure 651 was purchased from Ciba Inc. To prepare the 100% PEGDA solution, 1% (wt/vol) Irgacure 651, 0.5% (wt/vol) TEMPO free radical absorber, 0.5% (wt/vol) HMBS was added and sonicated for one hour. Gelatin methacrylate (GelMA) and lithium phenyl-2,4,6-trimethylbenzoylphosphinate (LAP) was synthesized as described previously.[39,40]

Device design and fabrication

Sectioned standard microscope slides (VWR) were cleaned and subsequently functionalized with 3-(trimethoxysilyl)propyl methacrylate (TMPSA, Sigma) as previously described.[32] Predefined 500 μm PDMS spacers were used to separate a methacrylated slide from a sacrificial platform, and this space was then filled with the PEGDA-based prepolymer solution. The gestalt microfabrication process is depicted in schematic form in Fig. 1. In our previous work, we have demonstrated the use of continuous optical-based 3D-printing to fabricate complex 3D structures with high aspect ratios in very short time scales.[41] The μCOP system (Fig. 1a) is comprised of 1) a UV light source (Omnicure 2000), 2) a digital micromirror device (DMD), 3) UV-grade projection optics (Edmunds Optics), a high precision computer controlled *x*–*y*–*z* stage (Newport 426/433 series), and a 4) CCD camera. The wavelength used to fabricate the PEGDA mold was 365 nm with a total output intensity of 2.4 W cm^{-2}.

Virtual masks of the VHMs were designed using Adobe Photoshop with increasing exposure corresponding to darker shades of gray. The images were imported into MATLAB (Mathworks) and made into transverse *z*-slices. The series of masks are then fed continuously corresponding to their respective *z*-positions, spatially patterning and curing the prepolymer solution. The full device consists of grayscale images in segments Fig. 1b, 1) ports, 2) T-junction, 3) micromixer unit, 4) culture chamber, and 5) an outlet. After each segment, the following segment's mask is aligned. The resulting polymerization of the five masks is a fully-featured, inverse-construct of our microfluidic device.

PDMS was then used in microcasting the PEGDA-based structural mold. PDMS is an attractive material for use in microfluidics due to its ease-of-use, material properties, and low costs, as demonstrated by its near ubiquity in microfluidic device fabrication. For the VHM, PDMS was created by using a 10 : 1 mixture of Sylgard 184 Silicone Elastomer and Sylgard 184 Curing Agent. Mixing of the PDMS was performed manually and then poured over the PEGDA molds to a controlled final thickness of 5 mm. In-solution bubbles from mixing were eliminated *via* vacuum at room temperature conditions for 1.5 hours. Curing of the PDMS casting of the PEGDA mold was done *via* convection oven at 100 °C for 1 hour.

Post-curing, the PDMS cast was extracted from the PEGDA mold and cleaned of any residual debris. Porting of the device's inlets and outlets was performed with a 16G needle (Becton-Dickinson). The PDMS cast and its paired glass slide were cleaned with deionized water and isopropanol, then air-

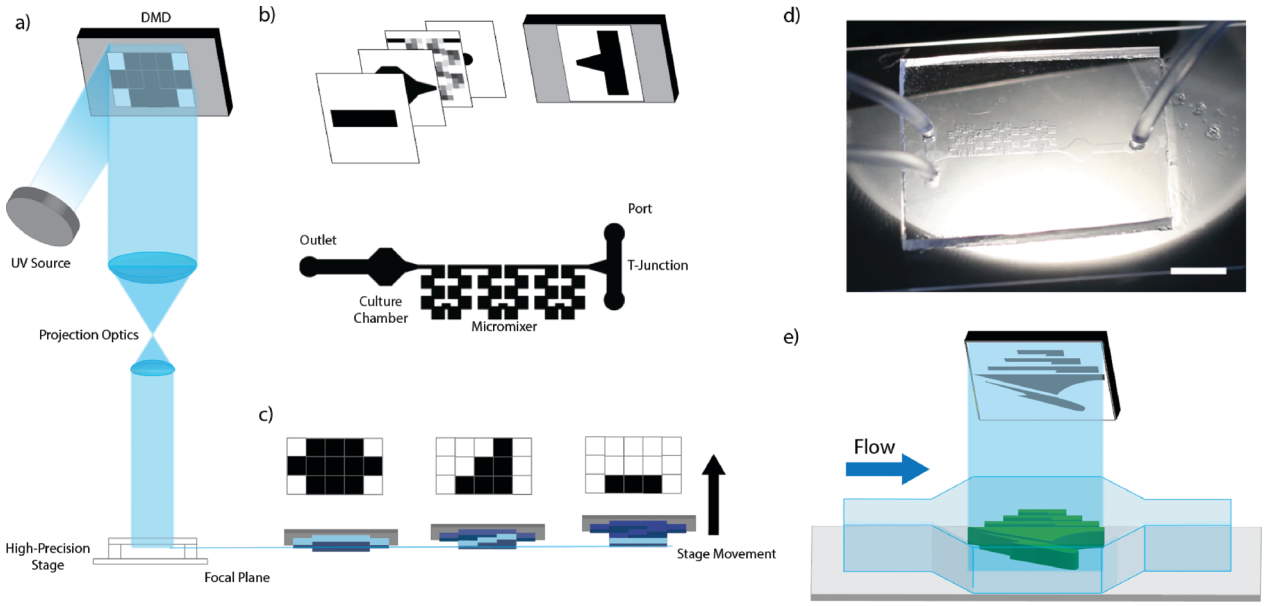

Fig. 1 a) Schematic of the μCOP system consisting of a UV source, DMD device to reflect user-specified patterns, projection optics to focus the light onto a prepolymer solution set on a high-precision stage. b) After producing a segment of the VHM device, the masks are changed and the device is stitched together using the *xy*-stage. c) Each segment is comprised of several virtual masks. The gray level determines the duration that the light is projected on a specific point, corresponding to taller structures. The light is modulated by changing masks corresponding to specified *z*-positions. d) Fabrication results of a VHM cast in PDMS, scale bar = 5 mm. Due to projection-based photopolymerization, the μCOP system allows for in-device printing e) of complex 3D structures when prepolymer solution is flowed in.

dried to remove residual water before undergoing RF-generated plasma cleaning in a Harrick Plasma PDC-002 plasma cleaner. The PDMS and glass were then bonded with firm manual pressing. Post-plasma-bonding, the device was heated on a hotplate at 85 °C for 8 minutes in order to finalize the bonding between the PDMS and glass. Once cooled, the device was visually inspected and underwent quality control checks for defects and leaks. An example device is presented in (Fig. 1d).

Mixing quantification

The device's mixing capability was evaluated by fluorescence imaging of on-chip mixing of a water-borne fluorescent dye. A Lucca Technologies GenieTouch™ dual-channel syringe pump was used to drive two 20 mL syringes, connected to the micromixer *via* 0.02″ ID Tygon tubing (Cole-Parmer) and 22 gauge blunt needles (Brico Medical). One 20 mL syringe contained a fluorescein isothiocyanate (FITC)-dextran fluorescent dye (Sigma, 20 000 MW) at 0.1 mg mL^{-1} in deionized water (DI) water, and the other 20 mL syringe contained DI water. No discernible cross-reactivity or auto-fluorescence was observed between the two solutions or with the PDMS device.

The fluorescence intensity within the VHM was visualized under a Leica inverted fluorescence microscope. Baseline measurements of the fluorescence intensity at the inlet and outlet of the micromixer were taken with the device fully-infused with deionized water and the 0.1 mg mL^{-1} FITC-dextran dye solution. All subsequent measurements of mixing conditions were normalized with respect to baseline FITC-dextran dye infusement. Multiple volumetric flow rates were explored, starting from 20 μL min^{-1} and subsequently doubling until 2400 μL min^{-1}. At each flow rate, the device was allowed to stabilize to steady state before taking measurements. Twenty images over the course of one second were taken. Fluorescence intensity profiles were produced using ImageJ and averaged over time.

In-device 3D scaffold printing

VHM devices were primed with 70% ethanol and subsequently treated with TMPSA solution. Samples were rinsed with 5 mL of DI water to ensure clearing of the device of any residual TMPSA. A syringe of 10% GelMA (wt/vol), 0.2% FITC-dextran (wt/vol), 0.4% LAP photoinitiator (wt/vol) in PBS and a second syringe of PBS was prepared. With the microfluidic micromixer deployed on the μCOP fabrication stage, the two solutions were injected at a volumetric flow rate of 640 μL min^{-1} each using the GenieTouch dual-channel syringe pump, for a total flow rate of 1280 μL min^{-1}. The solutions were injected for 30 seconds to allow the system to reach steady state, after which the syringe pump's flow was terminated, and the device outlet was clamped. The solution was allowed to settle for 15 seconds. To further demonstrate the capability of μCOP samples were fabricated within the VHM originally produced from the same system (Fig. 1e).

Cell culture and in-device cell encapsulation

C3H/10T1/2 murine mesenchymal progenitor cells were purchased from ATCC and cultured according to protocol provided by ATCC. 10T1/2 cells were cultured in Dulbecco's Modified Eagle Medium (DMEM, Gibco) supplemented with 10%

fetal bovine serum, heat inactivated (hyclone). Cells were maintained in a 37 °C incubator with 5% CO_2. Prior to encapsulation, cells were treated with CellTracker™ Green (ThermoFisher) per manufacturer's protocol. Prior to staining, cell culture media was aspirated and cells were washed using warm PBS. DMEM with CellTracker Green (1 : 1000) in DMEM without serum was added to culture flasks and incubated at 37 °C, 5% CO_2 for 30 minutes. Cells were harvested using 0.25% trypsin/EDTA and counted using general protocol. Cells were centrifuged at 210 RCF to produce a cell pellet and re-suspended to a concentration of 5×10^6 cells per mL in DMEM with 10% FBS and 1% penicillin–streptomycin. A 5 mL syringe was filled with the cell suspension and loaded on the GenieTouch dual syringe pump along with another 5 mL syringe filled with pre-warmed GelMA prepolymer solution. The prepolymer solution and cell suspension were both connected to each inlet of the VHM, the VHM was placed on the μCOP system and the solutions injected for 30 seconds to ensure steady state. The syringe pump flow was terminated, and the device outlet was clamped. The solution was allowed to settle for 30 seconds. Samples were exposed to patterned 365 nm light from the μCOP system within the fabrication chamber for 30 seconds and imaged with fluorescence microscopy.

Results and discussion

Fabrication result analysis

Three microfluidic micromixer molds of increasing complexity (Fig. 2a: 1×1-unit, 3×3-unit, 9×9-unit) were printed using the μCOP system. A set of 2D masks were created with 9 shades of gray, with the 1×1-unit requiring only one shade. For the 9×9-unit device, 9 shades are repeated 9 times, appearing once every 1/3 segment of the single unit. The micromixer segment of the microfluidic device was comprised of 48 masks. To ensure proper polymerization of the entire structure, a set of eight base layers was required to initialize polymerization for the entire structure. Each subsequent darker shade of gray was exposed for four more layers than the preceding lighter shade, arriving at a total of 48 masks.

The exposure time per layer was determined empirically to be 0.3 seconds to ensure that the fluid path fully formed with varied heights. Utilizing the *xyz* stage, the total microfluidic device was stitched from 9 exposures, three ports, a T-junction, three micromixers, the culture chamber, and an outlet. The total time to produce a single VHM mold was less than 5 minutes.

The PEGDA-based prepolymer solution, once fully-cured, proved to be a useful prototyping medium for PDMS micro-casting of our microfluidic device. 100% PEGDA's mechanical

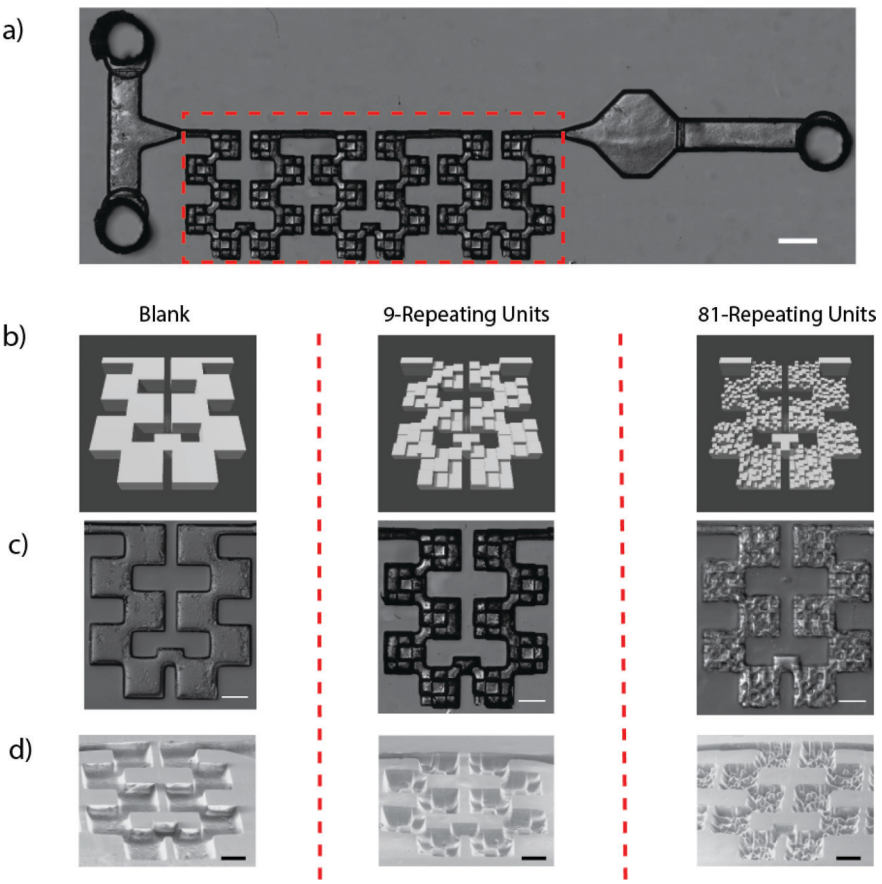

Fig. 2 Schematic of μCOP-enabled VHM device. a) DIC images of a full VHM device (scale bar = 1 mm). From left to right, blank, 9-repeating unit, and 81-repeating unit micromixer are shown, b) solid models, c) DIC images (scale bar = 500 μm), d) and SEM micrographs pitched at a 45 angle (scale bar = 500 μm).

stiffness[29] proved sufficient to survive the rigors of PDMS microcasting at elevated temperatures while accurately preserving critical device features. The final casting of the 1×1-unit, 3×3-unit, and 9×9-unit PDMS molds can be observed in stereo microscope and scanning electron microscopy (SEM) images of the PDMS castings of the VHM molds (Fig. 2b and c).

Structural design and simulation analysis

As a passive micromixer tends to have no moving parts beyond its fluidic driver, mixing must be accomplished by means of interfacing fluid streams with the device's geometry in such a way to enhance diffusion and/or create chaotic advection. In planar micromixers, the designer is by definition restricted to two dimensions, but operating in 3D allows for more variation within the same physical footprint. Here, we propose a variable height micromixer (VHM) that combines a T-junction with repeating zigzagging chains of block-like elements dubbed 'macro-squares,' with each macro-square spatially-patterned with grids of rectangular columns that range from 100 μm to 400 μm in height (Fig. 1). With a maximum device height of 500 μm, any given particle in the device is forced to not only navigate in 2D, but over and around obstacles of varying heights. These rectangular columns obstruct flow within the VHM, causing fluidic tumbling and chaotic advection that enhances mixing of fluids before their arrival in an octagonal fabrication chamber, where additional structures may then be constructed *via* μCOP.

Three VHM variations were numerically simulated using finite element method analysis. First, a control structure (designated '1×1-unit') was designed to emulate a planar micromixer set at a constant 500 μm in height throughout the device. The next iteration (designated '3×3-unit') introduced a 3×3 grid of 300 × 300 μm square columns of varying heights into every macro-square as described. The last level of complexity (designated '9×9-unit') was for each macro-square to have a 9×9 grid of 100 × 100 μm variable-height square columns, effectively a 3-fold increase in fluidic perturbation. These three variations were virtualized in 3D with the aid of computer modeling program AutoCAD (ESI† Fig. SI1), and mixing was simulated using commercial finite element software (COMSOL Multiphysics). First, the solutions for single-phase, incompressible laminar flow was applied throughout the entire geometry of each of the three VHM models for a wide variety of flow rates, with no-slip conditions at the sidewalls and the outlet pressure (p) set to zero. Second, the concentration profile of the simulated fluorescent dye was solved for using the previously-solved laminar flow solution. Additional assumptions include: 1) concentration of the simulated fluorescent dye did not affect dynamic viscosity and density of the water carrier fluid, 2) wall surface tension, gravitational forces, and body forces were considered negligible. Free tetrahedral meshes optimized for fluid dynamics were chosen for the VHMs, with the number of mesh elements ranging from approximately 146 K domain elements for the 1×1-unit model, to 1.2 M domain elements for the 9×9-unit model.

In characterizing the VHM, consideration must be given to the device's Reynolds number and Peclet number and how they change throughout the device due to the 3D nature of the device. They are governed by the equations:

$$\mathrm{Re} = \frac{\rho v D_{\mathrm{H}}}{\mu} \tag{1}$$

$$\mathrm{Pe} = \frac{v D_{\mathrm{H}}}{D} \tag{2}$$

where ρ is fluid density, v is linear flow rate, D_{H} is the characteristic dimension, μ is fluid dynamic viscosity, and D is the mass diffusion coefficient of the solute species. In rectangular-shaped microchannels, the characteristic dimension is equivalent to the hydraulic diameter, which is given by the equation:

$$D_{\mathrm{H}} = \frac{4A}{P} \tag{3}$$

where A is the cross-sectional area of the flow region, and P is the wetted perimeter, which is the perimeter of the cross-sectional area in contact with the aqueous medium.

From the model's geometry, the largest possible flow region barring the main fabrication chamber is the inlet region just before the tapered entry into the micromixing region, where the cross-sectional area is 5.00×10^{-7} m^2 and its corresponding D_{H} is 6.67×10^{-10} m. The smallest possible flow region among the VHMs can be found in select chokepoints of the 3×3-unit VHM, such as the overlapping area between the 6th and 7th macro-square (amounting to approximately a 5% overlap in linear footprint). The cross-sectional area for this region is 3.77×10^{-8} m^2, with a corresponding D_{H} of 1.81×10^{-4} m. We empirically determined that a total input volumetric flow rate of 1280 μL min^{-1} as the minimum rate at which effective mixing occurs. In Table 1, the local Reynolds numbers and Peclet numbers for the largest and smallest flow regions can be approximated based on model-derived estimates of maximum linear flow velocities at those regions (ESI† Movie SI1, SI3 and SI5).

The pressure drop experienced by laminar fluid flow in rectangular microchannels is governed by the Hagen–Poiseuille equation:

$$P = \frac{12 L \mu Q}{W H^3} \tag{4}$$

where Q is the volumetric flow rate, μ is fluid dynamic viscosity, and L, W, and H correspond to the length, width, and height of the microchannel. Due to the way the VHMs have abrupt changes in width and/or height over the course of the device, pressure drops for each device's mixing regions were determined analytically. At an input volumetric flow rate of 1280 μL min^{-1}, the pressure drop across the 1×1-unit,

Table 1 Approximations of local Reynolds and Peclet numbers for each VHM, at their largest and smallest flow regions

VHM type	Q [μL min^{-1}]	Re_{Inlet}	$Re_{Chokepoint}$	Pe_{Inlet}	$Pe_{Chokepoint}$
1×1-unit	1280	3.20×10^{-5}	1.37×10^{2}	0.339	1.45×10^{6}
3×3-unit	1280	3.20×10^{-5}	1.65×10^{2}	0.339	1.75×10^{6}
9×9-unit	1280	3.20×10^{-5}	2.34×10^{2}	0.339	2.48×10^{6}

3×3-unit, and 9×9-unit VHMs from the inlets to the outlet of the 30th macro-square were approximated to be 631 Pa, 3.48×10^{3} Pa, and 5.13×10^{3} Pa respectively (ESI† Fig. SI2).

Mixing analysis

In order to determine how well the VHM can homogeneously mix different solution streams, DI water and a solution of 0.1 mg mL^{-1} FITC-dextran were introduced *via* a T-junction at various flow rates. To better understand the effects of the VHM's on mixing of disparate fluids, fluorescent images were taken across the entire device and stitched into a gestalt image (Fig. 3a).

Across all three VHM variations, the collected data show that the two streams flow into the VHM and remain visually-distinct from each other while in the T-junction flow region. Mixing was negligible across all tested flow rates in this initial zone, likely due to the low residence time in the T-junction where only molecular diffusion dominates. Only once the combined fluid streams reached the zigzagging macro-squares did we begin to see the first signs of mixing. In the case of the 1×1-unit VHM, visually there is distinct separation between the two fluids until an input flow rate of 640 μL min^{-1}, where multiple slipstreams of DI and fluorescent dye begin to manifest. At an input flow rate of 640 μL min^{-1} (Fig. 3a), chaotic vortices begin to make their first appearances at the second macro-square, however a formation of slipstreams of DI and fluorescent dye are prevalent. It is not until 2400 μL min^{-1} does the 1×1-unit device achieve proper mixing prior to the outlet.

The 3×3-unit VHM improved mixing behavior compared to the 1×1-unit VHM; with numerous multi-lamellar streamlines forming by 160 μL min^{-1}, and significant chaotic advection behavior by 320 μL min^{-1}. By 640 μL min^{-1}, the fluid streams have mixed near 100% completeness at the outlet (30th macro-square). At 1280 μL min^{-1} and 2400 μL min^{-1} full mixing occurred by the 14th and 7th macro-square, respectively. The 9×9-unit VHM exhibits better advective mixing capability compared to the 3×3-unit VHM, with multi-lamellar streamlines forming by 80 μL min^{-1}, and significant chaotic advection behavior by 320 μL min^{-1}. At 640 μL min^{-1}, by the 24th macro-square, the fluid streams have mixed to 100% completeness. At 1280 μL min^{-1} and 2400 μL min^{-1}, full mixing occurred by the 12th and 10th macro-

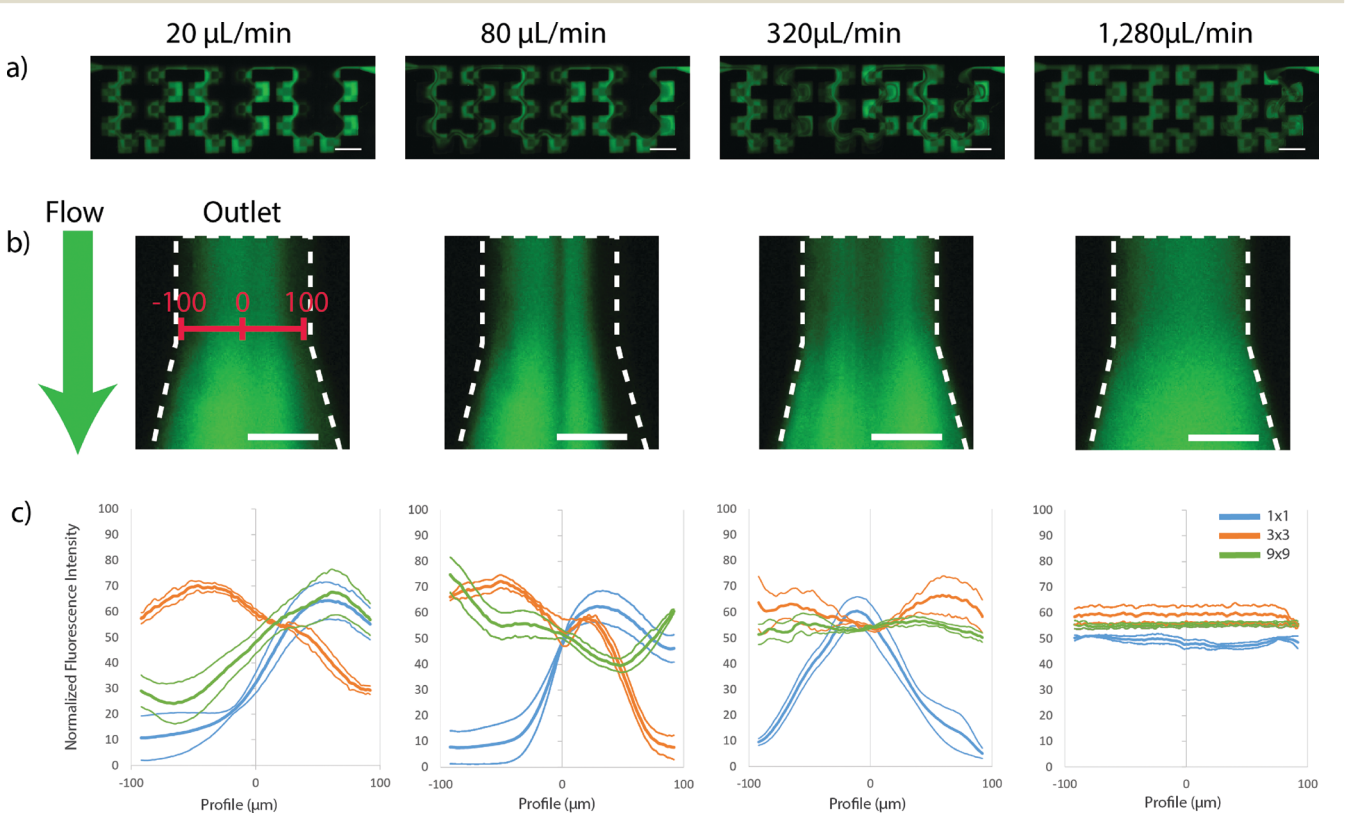

Fig. 3 Mixing behavior of VHM devices. a) Fluorescent images of a 3×3-unit VHM device across the total length of the zigzag micromixer (scale bar = 1 mm). b) Fluorescent images of the outlet of a 3×3-unit VHM at 40, 160, 640, and 2.4 ml min^{-1} (scale bar = 100 μm) where the c) intensity profiles were analyzed (blue = 1×1-unit, orange = 3×3-unit, green = 81 × 1×1-unit, n = 3).

squares, respectively. The experimentally-recorded concentration patterns of the VHMs agree well with the simulated data (ESI† Fig. SI3–SI4, Movie SI2, SI4 and SI6).

However, as we shift from the 1×1-unit to the 9×9-unit VHM, the decrease in feature size actually increases the variability of the fluidic path, thus increasing the variability in fluorescence intensity. This makes it difficult to accurately determine the level of mixing, thus higher magnification images were taken using a 10× object at the inlet and outlets of the three VHMs. An intensity profile was determined by drawing a line perpendicular to the flow direction across the outlet using ImageJ. 20 images were taken over 1 second, at 5 ms exposures and were averaged at each pixel across the profile. Fluorescence profiles across the outlets of three samples of each VHM geometry, 1×1 (blue), 3×3 (orange), and 9×9 (green), were taken (Fig. 3c). At 20 μL min^{-1} and 40 μL min^{-1} (ESI† 3c, Fig. 3c), we observe laminar flow with minimal streamline formation and lamellation. At 80 μL min^{-1} input flow rate, we begin to see the 9×9-unit exhibit the formation of local eddies and displaced streamlines, whereas the 3×3-unit and 1×1-unit VHMs do not. At 160 μL min^{-1}, the 9×9-unit continues to form larger vortices and increasingly more lamellations of fluorescent streamlines, whereas the 3×3-unit and 1×1-unit only just begin to shift their streamlines toward the midline of flow (ESI† 3c). At 320 μL min^{-1}, the 3×3-unit and 9×9-unit VHMs fluorescent lamellations begin to merge into homogeneity, whereas the 1×1-unit still exhibits a focusing of fluorescent streamlines toward the middle of the device, suggesting that the variable height geometries of the 3×3-unit and 9×9-unit VHMs are generating increased instances of mixing throughout the fluid path. By 1280 μL min^{-1}, the fluorescence profiles of the 3×3 and 9×9 stabilize into complete homogeneity, whereas the 1×1-unit still exhibited the incompletely-mixed multi-lamellar behavior that the 3×3-unit and 9×9-units had long since surpassed (Fig. 3c). Finally, at the final flow rate of 2400 μL min^{-1}, all three devices were fully mixed, indicating that even the 1×1-unit's smooth features were able to induce mixing by virtue of its zigzagging geometry. After empirically determining that both the 3×3-unit and 9×9-unit VHMs induced proper mixing by 1280 μL min^{-1}, we opted to utilize the 3×3-unit VHM at this flow rate for the demonstration of 3D-printing a cell-laden construct within a VHM.

In-chamber spatial patterning and cell encapsulation

To further the capabilities of the μCOP system beyond producing a mixing device, the ability to fabricate complex structures within the culturing chamber was explored. Pre-warmed syringes of 10% GelMA, 0.2% FITC-dextran, and 0.4% LAP and PBS was injected into the VHM at 640 μL min^{-1}, or a total flow rate of 1280 μL min^{-1} (Fig. 4a). After 30 seconds of flow, the outlet was clamped and the device was allowed to rest for 15 seconds. Images captured during the exposure of the prepolymer solution for 30 seconds indicated successful printing within the VHM (Fig. 4b; ESI† Movie SI1). The FITC-dextran/GelMA structure was imaged under fluorescence microscopy, which exhibited a faithful rendering of the 2D mask. Samples were cleaned using 0.25% trypsin/EDTA, filling the VHM, incubating samples for 5 minutes at 37 °C and were rinsed with DI water. Samples were retreated with TMPSA solution for 30 minutes and printed in again, demonstrating the ability to reuse the VHM as necessary. Whereas several 3D-printing technologies, including stereolithography[14] and extrusion-based[19,22,42] have produced functional microfluidic devices for 2D and 3D culture[24] and mixing,[6] these devices do not allow for post-fabrication design of simple or complex architecture. That is, the design of the microfluidic device will also dictate and limit the scope of studies that can be performed *in situ*. The μCOP system as used in this report enables users to print complex 3D geometries within a completed microfluidic device, potentially allowing for further studies in how cell interaction with materials are affected by flow. The VHM system along with *in situ* polymerization of prepolymer solutions can be extended to study cell interactions with gradients of materials, localized changes in stiffness by controlling exposure time, or the introduction of multiple materials.

Ultimately, the purpose of the VHM was designed to limit the amount of time the cells were exposed to the prepolymer solution prior to cell encapsulation. A 5 mL syringe of 10T1/2 cell suspension (5×10^6 cells per ml), treated with CellTracker Green and a 5 mL syringe of 10% GelMA, 0.4% LAP solution placed on the syringe pump and was injected into the VHM at 640 μL min^{-1}, or a total flow rate of 1280 μL min^{-1} (Fig. 4a). The mixed cell suspension/prepolymer solution within the fabrication chamber was subjected to an exposure of 365 nm light from a digital mask comprised of hexagons for 30 seconds. 10T1/2 cells were successfully encapsulated *in situ* within a spatially patterned hexagonal pattern in the GelMA construct and excess cells and prepolymer solution were gently flushed with DMEM with 10% FBS before imaging at 10 μL min^{-1} from the outlet for 5 minutes. Cells premixed 1 : 1 within a 1.5 mL centrifuge tube and polymerized on a methacrylated slide (Fig. 4c) were compared with a cell/prepolymer solution mixed using the VHM (Fig. 4d). Pattern fidelity was maintained and cells were successfully encapsulated utilizing the μCOP system in constructs printed using manual mixing and VHM mixing methods. The presence of cell aggregates in the VHM mixed samples may indicate a gentler mixing. Upstream agitation of the syringes was not employed prior to mixing through the VHM and may be necessary for future cell studies utilizing this method, especially with higher cell concentration suspensions. Cell viability studies, along with long-term culture under fluidic conditions are reserved for future studies. By demonstrating the ability to both produce a complex VHM device and to spatially pattern cells in complex geometries post-fabrication within the device, the μCOP system can be a useful platform to produce cost-effective microfluidic devices that can serve multiple purposes and to study the effects of fluid flow on complex 3D-printed tissues.

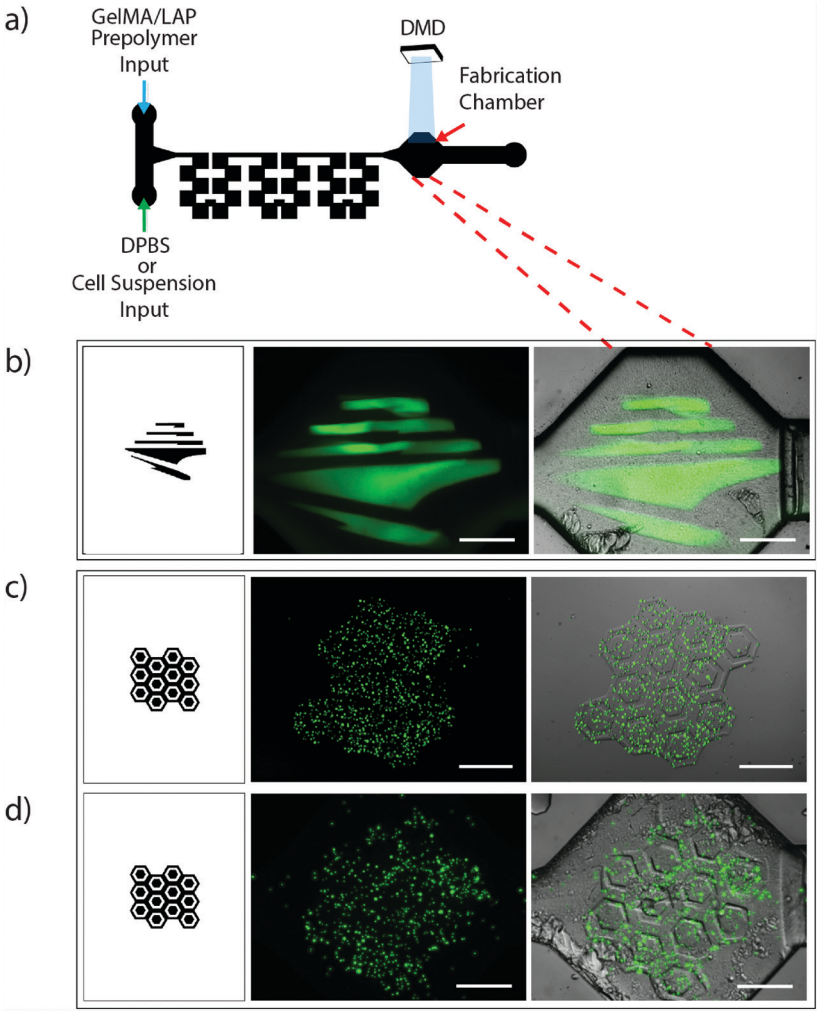

Fig. 4 Fabrication within VHM. a) A schematic of the VHM device with the 10% GelMA, 0.4% LAP prepolymer solution connected to one inlet and DPBS or a 10T1/2 cell suspension connected to the other. The solutions were injected through the VHM at a total flow rate of 1280 μL min^{-1} to induce mixing. The mixed prepolymer solution was subjected to a digital mask reflecting 365 nm light. b) A fluorescent (left) and composite image (right) of the UCSD logo 3D printed within the VHM fabrication chamber. c) Fluorescent and composite images of a biomimetic hepatic lobule structure was printed with premixed CellTracker Green cells and prepolymer solution (1 : 1) compared to d) 10T1/2 cells mixed against the prepolymer solution within the VHM device.

Conclusions

In this report, we describe the ability to efficiently mix two fluids within a microfluidic device such that a tissue scaffold can be printed *in situ* within the device. The variable-height features within each of the 3×3-unit and 9×9-unit VHMs induced better mixing capability when compared to the 1×1-unit VHM. The experimental data for each of the VHMs show good agreement with the simulated results for our tested range of flow rates, with a Reynolds number range of $3.2 \times 10^{-5} < Re < 234$ across the slowest and fastest regions of the VHMs, respectively. The pressure drop range was 631 Pa $< \Delta P <$ 5130 Pa for the 1×1-unit and 9×9-unit VHMs, respectively. A dual-channel syringe pump was used to drive the 10T1/2 cell suspension and GelMA prepolymer solution into the device, where hierarchically-patterned features induced passive mixing of the two substances such that a three-dimensional, cell-encapsulating tissue scaffold could be fabricated out of the mixed solutions. We believe that low-flow rate microfluidic mixers of this type can be used in a wide variety of applications where in-device mixing of reagents is preferable to pre-mixing external to the device, such as in 3D-printing, where mixing live cells with prepolymer solutions may be deleterious. Longer term goals involve optimizing the micromixer design for improved mixing efficacy, and tailoring the concept for application-specific needs that require micromixing and *in situ* 3D-printing. The ability to print 3D architectures within a microfluidic chamber, along with the ability to spatially pattern cells greatly extends the capabilities and future direction of microfluidic device design.

Acknowledgements

This project received support from the Department of Defense (W81XWH-14-1-0522), California Institute for Regenerative

Medicine (RT3-07899) and National Science Foundation (CMMI-1332681 and CMMI-1547005). We also acknowledge the UCSD Neuroscience Microscopy Shared Facility grant P30 NS047101 for use of confocal imaging and thank Dr. Darren Lipomi for allowing the use of his plasma cleaning system.

References

1 P. Yager, T. Edwards, E. Fu, K. Helton, K. Nelson, M. R. Tam and B. H. Weigl, *Nature*, 2006, **442**, 412–418.
2 M. Toner and D. Irimia, *Annu. Rev. Biomed. Eng.*, 2005, **7**, 77–103.
3 A. K. Yetisen, M. S. Akram and C. R. Lowe, *Lab Chip*, 2013, **13**, 2210–2251.
4 G. M. Whitesides, *Nature*, 2006, **442**, 368–373.
5 Y. K. Suh and S. Kang, *Micromachines*, 2010, **1**, 82–111.
6 C.-Y. Lee, C.-L. Chang, Y.-N. Wang and L.-M. Fu, *Int. J. Mol. Sci.*, 2011, **12**, 3263–3287.
7 S.-J. Park, J. K. Kim, J. Park, S. Chung, C. Chung and J. K. Chang, *J. Micromech. Microeng.*, 2004, **14**, 6–14.
8 R. H. Liu, M. A. Stremler, K. V. Sharp, M. G. Olsen, J. G. Santiago, R. J. Adrian, H. Aref and D. J. Beebe, *J. Microelectromech. Syst.*, 2000, **9**, 190–197.
9 V. Viktorov and M. Nimafar, *J. Micromech. Microeng.*, 2013, **23**, 055023.
10 C. M. B. Ho, S. H. G. Ng, K. H. H. Li and Y.-J. Yoon, *Lab Chip*, 2015, **15**, 3627–3637.
11 E. C. Spivey, B. Xhemalce, J. B. Shear and I. J. Finkelstein, *Anal. Chem.*, 2014, **86**, 7406–7412.
12 A. K. Au, W. Lee and A. Folch, *Lab Chip*, 2014, **14**, 1294–1301.
13 E. C. Spivey, B. Xhemalce, J. B. Shear and I. J. Finkelstein, *Anal. Chem.*, 2014, **86**, 7406–7412.
14 A. K. Au, W. Lee and A. Folch, *Lab Chip*, 2014, **14**, 1294–1301.
15 O. H. Paydar, C. N. Paredes, Y. Hwang, J. Paz, N. B. Shah and R. N. Candler, *Sens. Actuators, A*, 2014, **205**, 199–203.
16 C. I. Rogers, K. Qaderi, A. T. Woolley and G. P. Nordin, *Biomicrofluidics*, 2015, **9**, 16501.
17 A. I. Shallan, P. Smejkal, M. Corban, R. M. Guijt and M. C. Breadmore, *Anal. Chem.*, 2014, **86**, 3124–3130.
18 K. G. Lee, K. J. Park, S. Seok, S. Shin, D. H. Kim, J. Y. Park, Y. S. Heo, S. J. Lee and T. J. Lee, *RSC Adv.*, 2014, **4**, 32876–32880.
19 V. Saggiomo and A. H. Velders, *Adv. Sci.*, 2015, **2**, 1–5.
20 C. Chen, Y. Wang, S. Y. Lockwood and D. M. Spence, *Analyst*, 2014, **139**, 3219–3226.
21 K. B. Anderson, S. Y. Lockwood, R. S. Martin and D. M. Spence, *Anal. Chem.*, 2013, **85**, 5622–5626.
22 D. B. Kolesky, R. L. Truby, A. S. Gladman, T. A. Busbee, K. A. Homan and J. A. Lewis, *Adv. Mater.*, 2014, **26**, 3124–3130.
23 D. B. Kolesky, R. L. Truby, A. S. Gladman, T. A. Busbee, K. A. Homan and J. A. Lewis, *Adv. Mater.*, 2014, **26**, 3124–3130.
24 S. N. Bhatia and D. E. Ingber, *Nat. Biotechnol.*, 2014, **32**, 760–772.
25 Y. Liu, C. Chen, S. Summers, W. Medawala and D. M. Spence, *Integr. Biol.*, 2015, **7**, 534–543.
26 K. G. Lee, K. J. Park, S. Seok, S. Shin, D. H. Kim, J. Y. Park, Y. S. Heo, S. J. Lee and T. J. Lee, *RSC Adv.*, 2014, **4**, 32876.
27 S. P. Grogan, P. H. Chung, P. Soman, P. Chen, M. K. Lotz, S. Chen and D. D. D'Lima, *Acta Biomater.*, 2013, **9**, 7218–7226.
28 J. W. Lee, K.-J. Kim, K. S. Kang, S. Chen, J.-W. Rhie and D.-W. Cho, *J. Biomed. Mater. Res., Part A*, 2013, **101A**, 1865–1875.
29 P. Soman, J. A. Kelber, J. W. Lee, T. N. Wright, K. S. Vecchio, R. L. Klemke and S. Chen, *Biomaterials*, 2012, **33**, 7064–7070.
30 S. Suri, L.-H. Han, W. Zhang, A. Singh, S. Chen and C. E. Schmidt, *Biomed. Microdevices*, 2011, **13**, 983–993.
31 A. P. Zhang, X. Qu, P. Soman, K. C. Hribar, J. W. Lee, S. Chen and S. He, *Adv. Mater.*, 2012, **24**, 4266–4270.
32 P. Soman, P. H. Chung, A. P. Zhang and S. Chen, *Biotechnol. Bioeng.*, 2013, **110**, 3038–3047.
33 X. Qu, W. Zhu, S. Huang, Y.-S. Li, S. Chien, K. Zhang and S. Chen, *Biomaterials*, 2013, **34**, 9812–9818.
34 T. Q. Huang, X. Qu, J. Liu and S. Chen, *Biomed. Microdevices*, 2014, **16**, 127–132.
35 K. Kim, W. Zhu, X. Qu, C. Aaronson, W. R. McCall, S. Chen and D. J. Sirbuly, *ACS Nano*, 2014, **8**, 9799–9806.
36 M. Gou, X. Qu, W. Zhu, M. Xiang, J. Yang, K. Zhang, Y. Wei and S. Chen, *Nat. Commun.*, 2014, **5**, 3774.
37 K. C. Hribar, D. Finlay, X. Ma, X. Qu, M. G. Ondeck, P. H. Chung, F. Zanella, A. J. Engler, F. Sheikh, K. Vuori and S. C. Chen, *Lab Chip*, 2015, **15**, 2412–2418.
38 W. Zhu, J. Li, Y. J. Leong, I. Rozen, X. Qu, R. Dong, Z. Wu, W. Gao, P. H. Chung, J. Wang and S. Chen, *Adv. Mater.*, 2015, **27**, 4411–4417.
39 J. W. Nichol, S. T. Koshy, H. Bae, C. M. Hwang, S. Yamanlar and A. Khademhosseini, *Biomaterials*, 2010, **31**, 5536–5544.
40 B. D. Fairbanks, M. P. Schwartz, C. N. Bowman and K. S. Anseth, *Biomaterials*, 2009, **30**, 6702–6707.
41 A. P. Zhang, X. Qu, P. Soman, K. C. Hribar, J. W. Lee, S. Chen and S. He, *Adv. Mater.*, 2012, **24**, 4266–4270.
42 J. S. Miller, K. R. Stevens, M. T. Yang, B. M. Baker, D. H. Nguyen, D. M. Cohen, E. Toro, A. A. Chen, P. A. Galie, X. Yu, R. Chaturvedi, S. N. Bhatia and C. S. Chen, *Nat. Mater.*, 2012, **11**, 768–774.

